Nanoscale

Supplementary Materials

Deep Learning-Driven Forward and Inverse Design of Nanophotonic Nanohole Arrays: Streamlining Design for Tailored Optical Functionalities and Enhancing Accessibility†

Tasnia Jahan[a], Tomoshree Dash[a], Shifat E Arman[b], Reefat Inum [c], Sharnali Islam[a], Lafifa Jamal[b], Ahmet Ali Yanik[c] and Ahsan Habib* [a,d]

1 Supplementary Text 1: Benchmarking experimental spectrum with numerical simulation

We validate our FDTD simulation of the hexagonal nanohole array device by benchmarking it against the results published by Conteduca et al.[1]. The device consists of a hydrogenated amorphous silicon dioxide film with parameters that match those reported in the literature: 110 nm thickness, 60 nm radius, and 480 nm periodicity. As shown in Figure S1b, our FDTD simulations closely mirror the experimental reflection spectra after calibration, confirming the accuracy and reliability of our simulation model.

Subsequently, leveraging this calibrated model, we extended our study to investigate different materials, specifically gold (Au) and silver (Ag). For the optical constants of Au, we used the data from Johnson and Christy[2], while for Ag, we used the Palik data[3] for the 0-2 μm range.

We also benchmarked the nanohole array with a square lattice configuration, achieving consistent agreement between the FDTD simulated transmittance and the experimental data using identical parameters (thickness: 120 nm, radius: 140 nm, and periodicity: 520 nm). As shown in Figure S1a, the experimental spectrum closely matches the simulation, underscoring the accuracy of our model. This model was then applied to generate transmission spectra for gold and silver nanohole arrays.

2 Supplementary Text 4: Data Quality and Diversity

2.1 Data Quality

Our dataset contains no missing values or duplicate rows, ensuring the integrity of the data. Outlier detection using the Interquartile Range (IQR) method indicates no outliers in the structural parameters, affirming the reliability of the data. The IQR method is a statistical technique used to detect outliers in a dataset. It involves calculating the range between the first quartile (Q1) and the third quartile (Q3) of the data, which represents the middle 50% of the dataset. An outlier is defined as

[a] Department of Electrical and Electronic Engineering, University of Dhaka, Dhaka-1000, Bangladesh; E-mail: mahabib@du.ac.bd
[b] Department of Robotics and Mechatronics Engineering, University of Dhaka, Dhaka-1000, Bangladesh
[c] Department of Electrical and Computer Engineering, University of California, Santa Cruz, CA-95064, United States of America
[d] Dhaka University Nanotechnology Center, University of Dhaka, Dhaka-1000, Bangladesh

any data point that falls below $Q1 - 1.5 \times \text{IQR}$ or above $Q3 + 1.5 \times \text{IQR}$. This method helps identify values that are significantly lower or higher than the rest of the data, thereby ensuring the integrity and reliability of the dataset.

$$\text{IQR} = Q3 - Q1 \tag{1}$$

A point is considered an outlier if it is:

$$\text{Less than } Q1 - 1.5 \times \text{IQR} \quad \text{or} \quad \text{greater than } Q3 + 1.5 \times \text{IQR} \tag{2}$$

2.2 Diversity of Data

We varied key structural parameters extensively: film thickness (100-150 nm), hole radius (50-100 nm for hexagonal, 100-150 nm for square), and periodicity (475-525 nm). These ranges fall within practical nanohole device dimensions reported in the literature, providing a diverse and representative dataset for training[1,4]. The distribution plots for these parameters and transmittance data points further confirm the dataset's robustness (Figure S9).

3 Supplementary Text 3: Forward and inverse model architecture and training

In Figure S3, it's evident that the training and validation losses decrease as we continue training our forward model. We observe that the model's improvement becomes very slow after 100 epochs. After 1500 epochs, the training MSE converges to an approximate value of 3.12×10^{-4}, while the validation MSE stabilizes around 4.81×10^{-4}. In learning curves of inverse models, we can see fluctuations at the beginning as the model adjusts to the training data, followed by a gradual decrease in loss as the model refines its parameters to better fit the data (Figure S5a). This decreasing trend indicates that our models are effectively capturing the underlying patterns in the training data. For the validation losses, as depicted in Figure S5b we assess how well our models generalize to unseen data. The training losses of the tandem network stabilize at 1.97×10^{-3}. On the other hand, validation losses stabilize at 5.66×10^{-3}. This indicates that our model is not only learning well from the training data but also generalizing effectively to new, unseen samples.

4 Supplementary Text 4: Comparison of tandem network prediction against true values in the test set

In the inverse prediction, after training the tandem neural network, the 666 groups of spectra from the testing dataset are fed into the network. The network then predicts the parameters: thickness (T), radius (R), and periodicity (P), which are subsequently compared with the original values employed to generate the spectra (Figures S7 and S8). As a guiding reference, the blue line represents y = x. The predicted values for T, R, and P closely follow the trend of y = x implying the predictions are very close to real values.

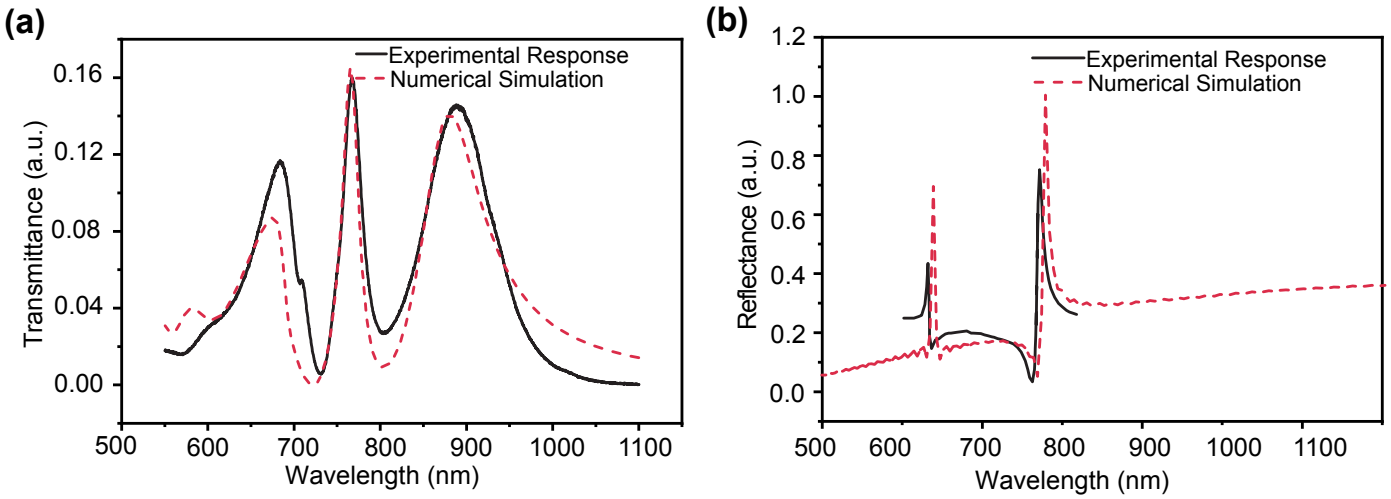

Fig. S1 Transmission spectrum from experiment and FDTD simulations (a) Square lattice with gold film, (b) Hexagonal lattice with a-SiOx:H film. Experimental data (red curve) used for benchmarking is adapted from Conteduca et al.[1].

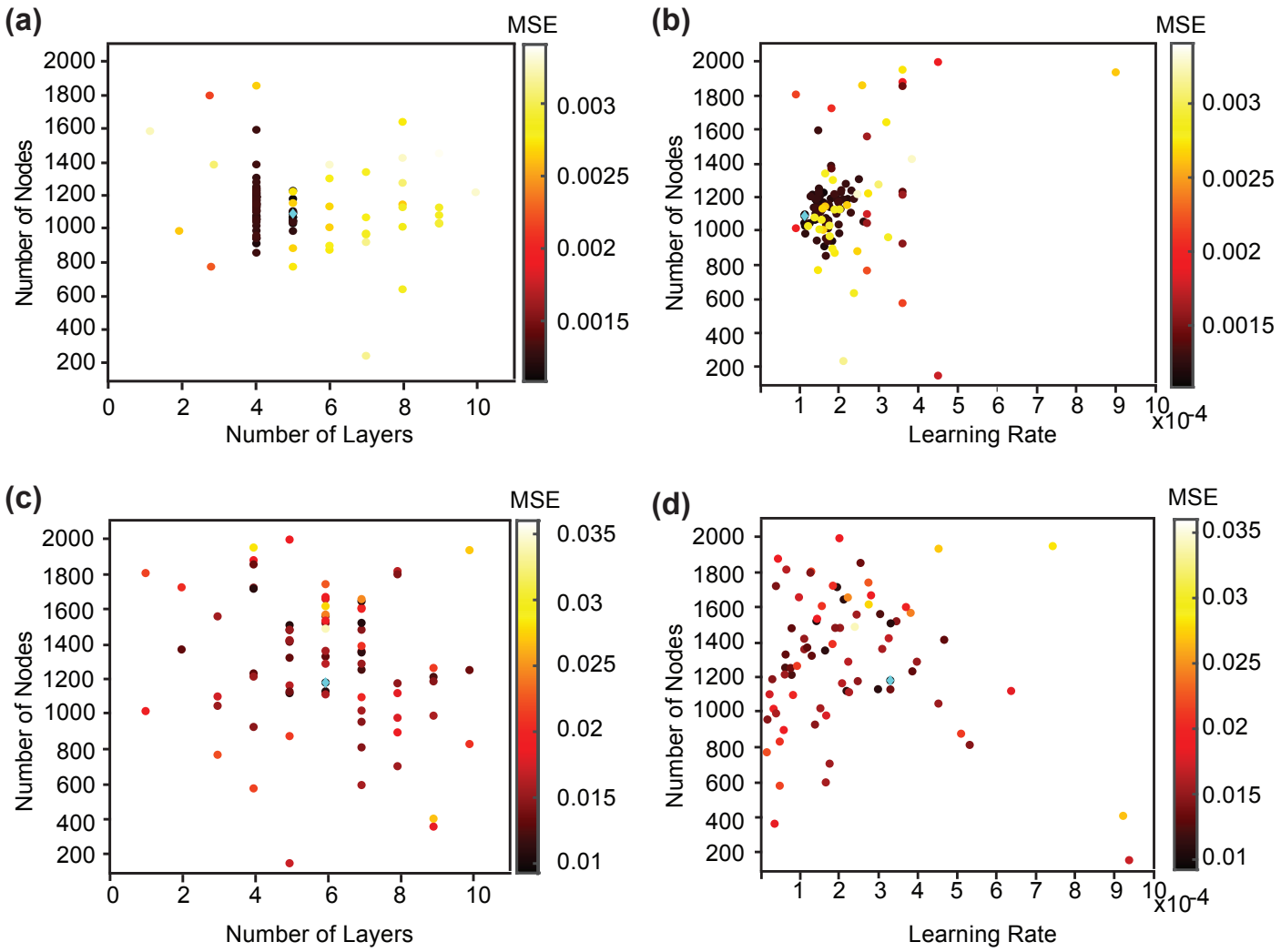

Fig. S2 (a) Scatter plot illustrating the relationship between Mean Squared Error (MSE) and the (a) number of layers and nodes in the forward network, the optimum architecture is 5 layers and 1080 nodes with lowest MSE of 0.0012 indicated by a cyan diamond, (b) learning rate and nodes in the forward network, the optimum hyperparameters are 1080 nodes and learning rate of 0.00011 with lowest MSE of 0.0012 marked with a cyan diamond, (c) number of layers and nodes in the forward network, the optimum architecture is 6 layers and 1180 nodes with lowest MSE of 0.0092 indicated by a cyan diamond. (d) learning rate and nodes in the inverse network, the optimum hyperparameters are 1180 nodes and learning rate of 0.000325 with lowest MSE of 0.0092 marked with a cyan diamond

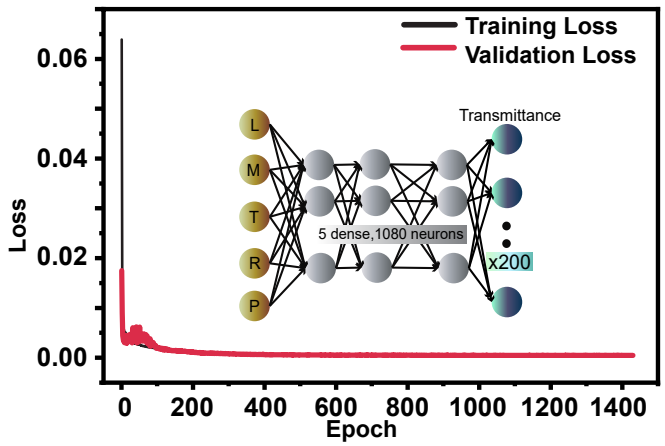

Fig. S3 Optimized forward neural network architecture and learning curves for spectrum prediction.

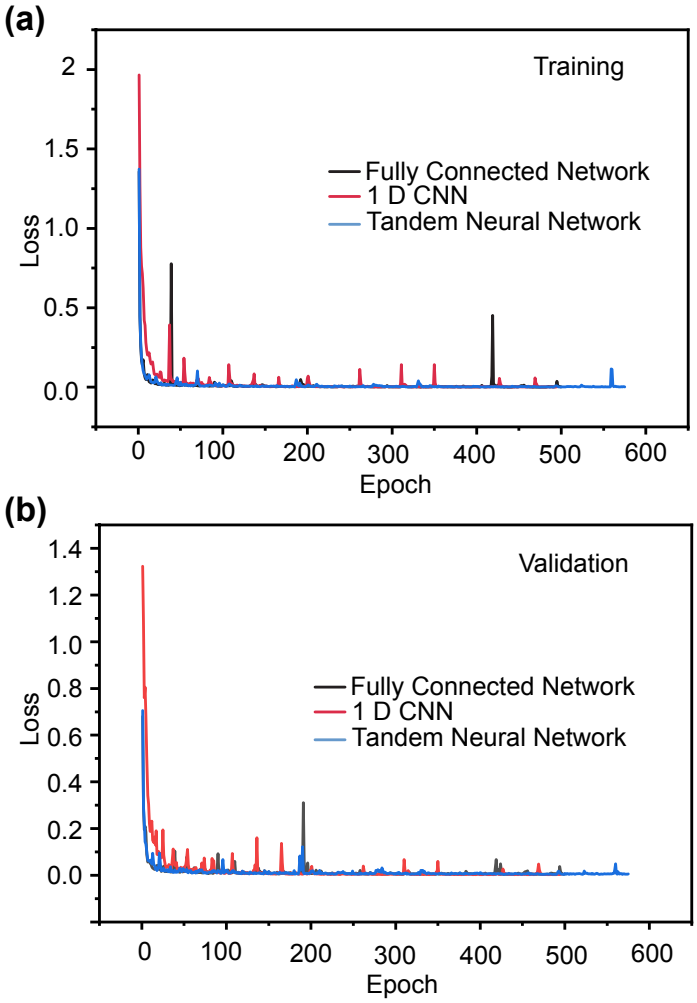

Fig. S4 Training and validation losses of the fully connected network, 1-D Convolutional neural network, and Tandem neural network for inverse design of nanohole arrays. (a) Training loss and (b) Validation loss are depicted for each network architecture.

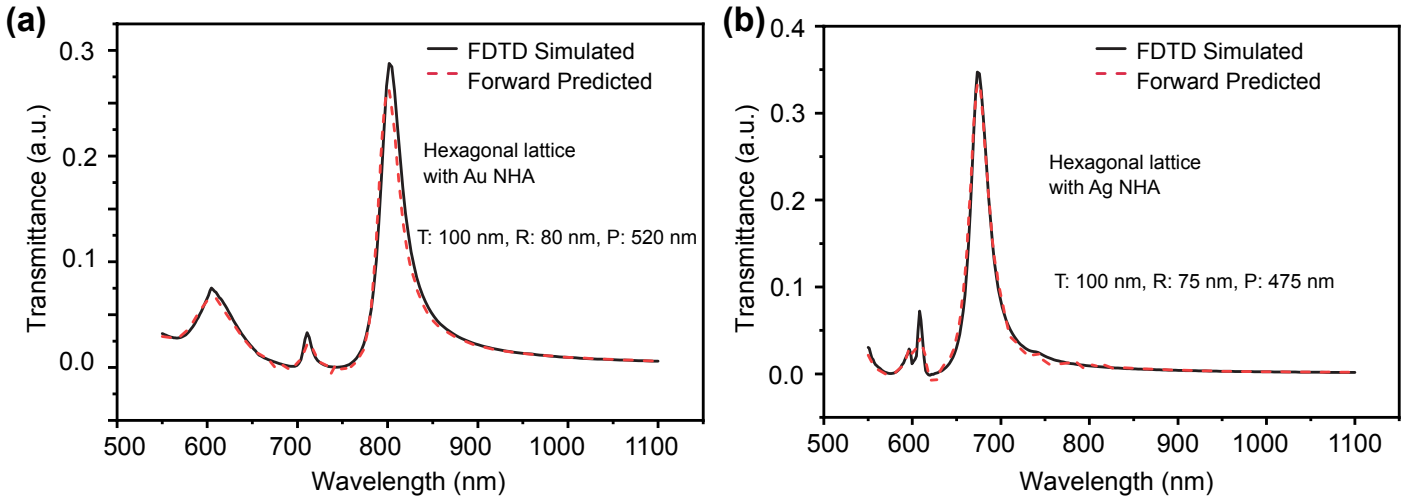

Fig. S5 Comparison between FDTD simulated spectra and Forward predicted spectra for (a) hexagonal lattice with Au film and (b) hexagonal lattice with Ag film.

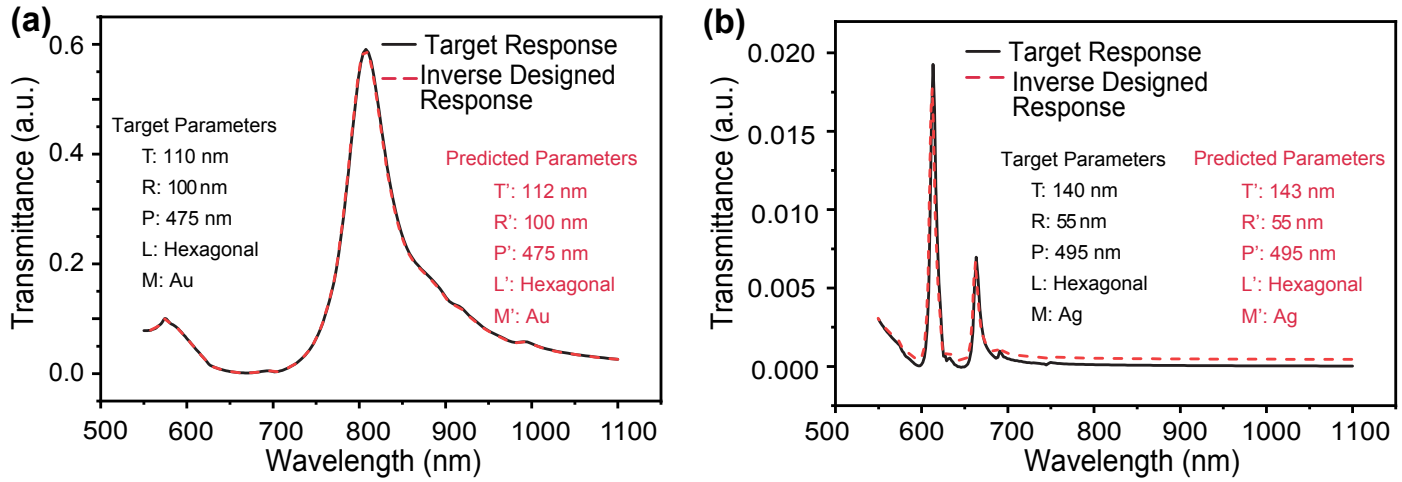

Fig. S6 Inverse design results for target spectrum randomly chosen from the test dataset. (a) Hexagonal lattice with Au film. (b) Hexagonal lattice with Ag film. Black solid lines show the target transmittance and red dashed lines show the corresponding transmission spectra by conducting FDTD calculation using the predicted structural parameters. Predicted parameters are labeled red and target parameters are labeled black on the figures

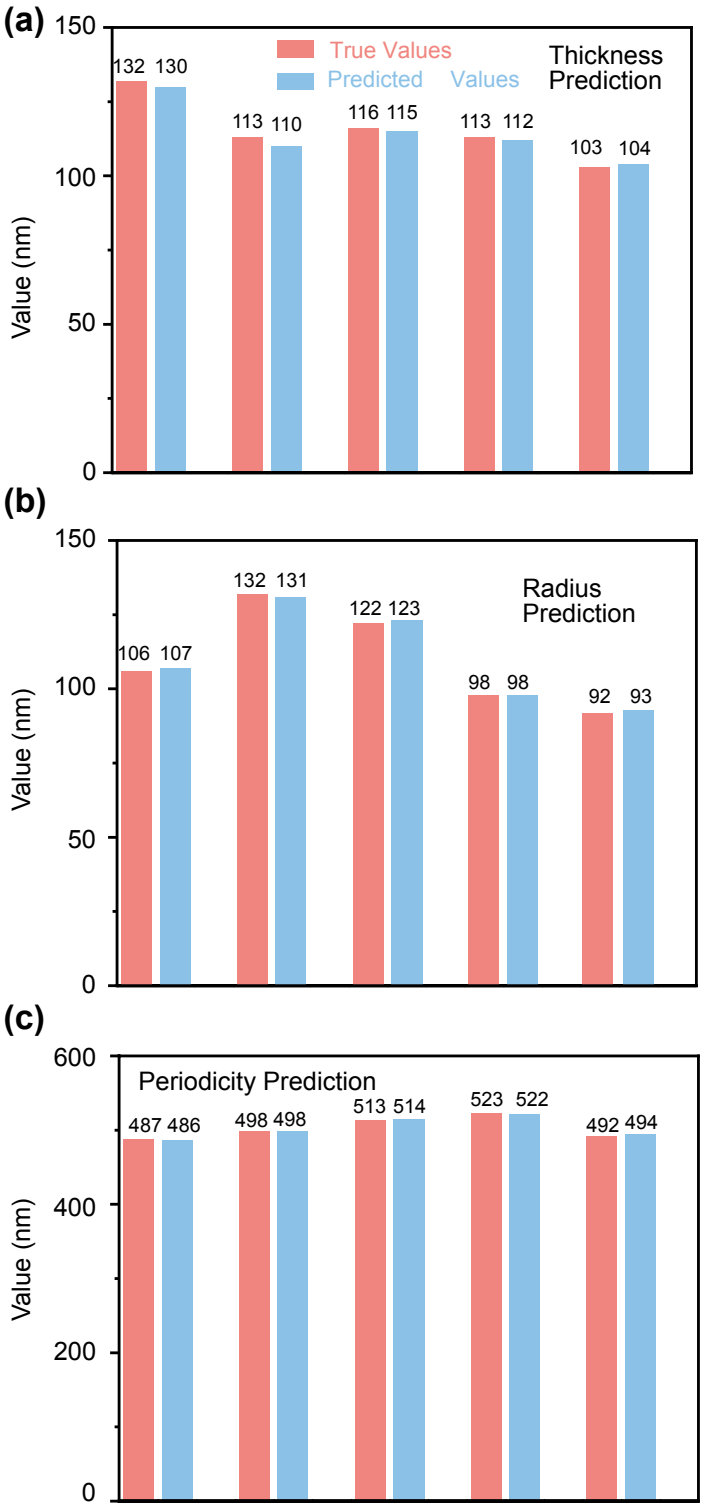

Fig. S7 Generalization Test Results of the Tandem Neural Network for Inverse Design. Comparison between original and predicted values of (a) Thickness, (b) Radius, (c) Periodicity. The close agreement between the retrieved geometrical values and the original values demonstrates the reliability of the trained tandem network for inverse design, even for samples outside the dataset.

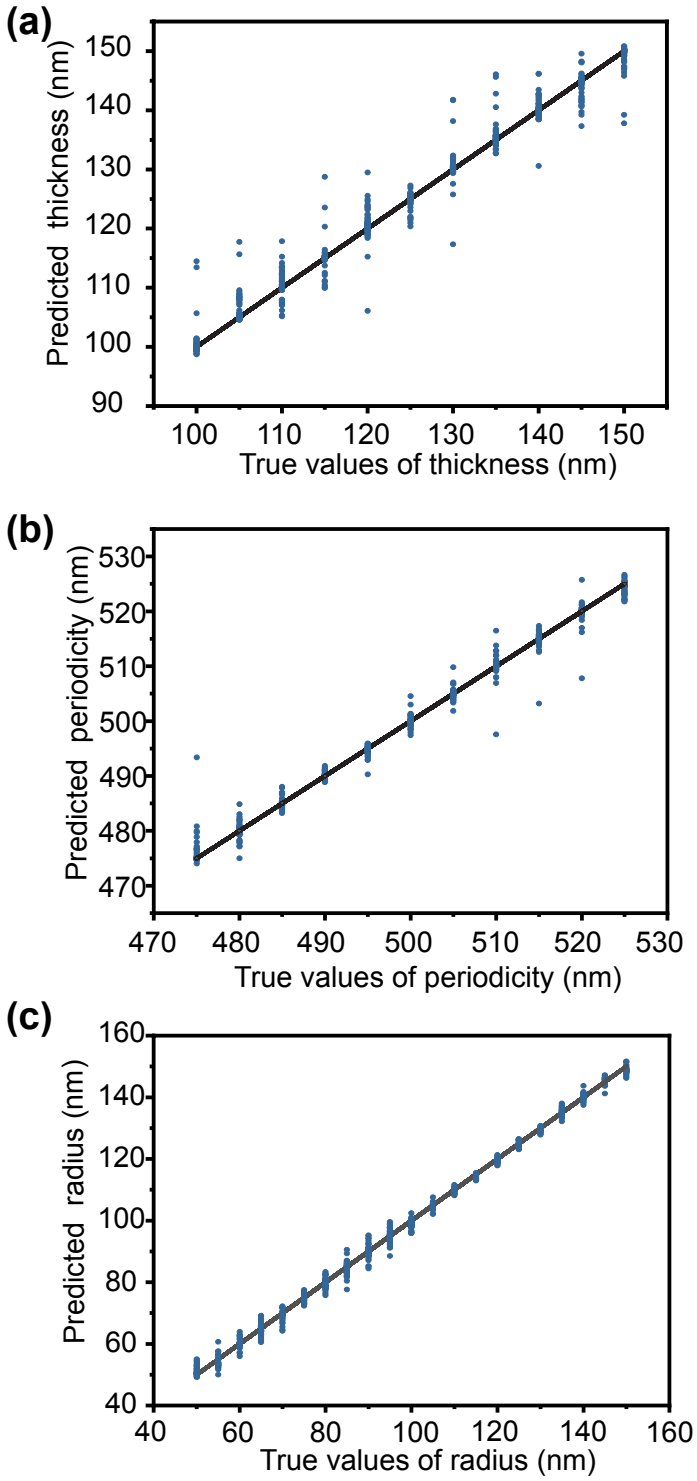

Fig. S8 Scatter plots of inverse predicted parameters for Tandem Neural Network : (a) thickness (b) radius and (c) periodicity, with respect to actual parameters.

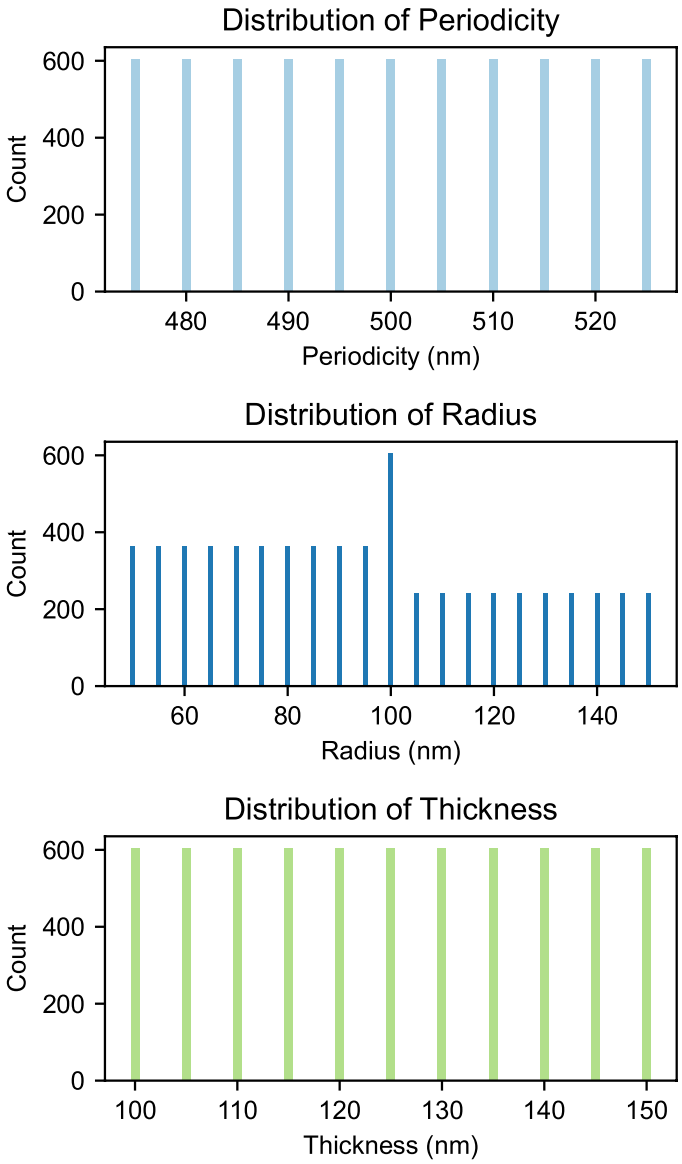

Fig. S9 Distribution of three critical parameters in the dataset used for training the deep learning model for nanohole array design.

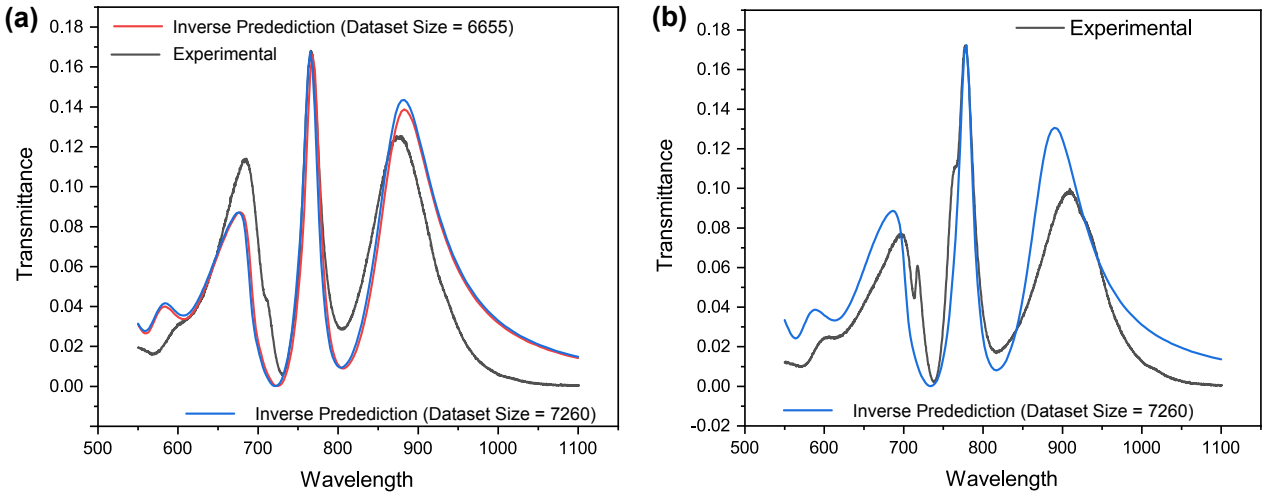

Fig. S10 (a) Comparison of experimental transmittance data for square Au NHA with deep neural network (DNN) predicted transmittance data for two different dataset sizes. The experimental data is shown in black, while the DNN-predicted data for dataset sizes of 6655 and 7260 are depicted in red and blue, respectively. (b) To further validate our model, we performed an additional validation using another experimental dataset. Our neural network predictions align well with the experimental spectrum. The target parameters are T: 120 nm, R: 140 nm, P: 530 nm, L: Square, M: Au. For the dataset size of 7260, the predicted parameters are T': 121 nm, R': 141 nm, P': 530 nm, L': Square, M': Au.

Table S1 Frequency of transmission spectra values for different types of nanohole arrays

Transmission Interval	Hexagonal Au	Hexagonal Ag	Hexagonal a-SiOx:H	Square Au	Square Ag
0-0.0001	3.67%	5.37%	0.0027%	0.9%	0.7%
0.0001-0.001	21%	23%	0.02%	3.32%	4.6%
0.001-0.01	42%	38%	0.13%	31.35%	35%
0.01-0.1	29%	29%	0.4%	64%	60%
0.1-1	4.4%	5.3%	99.4%	0.27%	0.13%

Table S2 Details of Training Parameters

Initializer	Weight: Uniform, Bias: Zeros
Activation Function	Hidden Layer: ReLU, Output Layer: Linear (Regression) and Softmax (Classification)
Loss	MSE (Forward Model), MSE and Sparse Categorical Cross-Entropy (Inverse Model)
Optimizer	Adam
Learning Rate	0.00011 (Forward Model), 0.000325 (Inverse Model)
Batch Size	128
Early Stopping	Yes

Table S3 Hyperparameter Optimization of 1D CNN. The table shows various trials with different combinations of convolutional layers, filter numbers, dense layers, node numbers, and learning rates. The optimal CNN configuration is chosen based on the lowest Mean Squared Error (MSE), which is observed in trial 16.

No. of trials	MSE	No. of Convolutional Layers	Filter numbers	No. of Dense Layers	Node Numbers	Learning Rate
1	0.0154	3	16, 32, 128	7	1350	0.00012
2	0.0194	6	16, 16, 128, 256, 32, 64	5	1087	0.0000142
3	0.016	2	16, 64	5	1843	0.0000584
4	0.028	1	128	10	700	0.00009
5	0.0354	5	16, 128, 16, 32, 256	8	731	0.00045
6	0.0086	6	16, 256, 32, 64, 32, 32	6	1166	0.00028
7	0.0168	3	16, 16, 16	7	1684	0.0007
8	0.0135	4	16, 128, 16, 128	8	800	0.0006
9	0.0148	1	32	6	1956	0.00024
10	0.0247	6	16, 16, 256, 64, 32 , 256	2	1243	0.000035
11	0.0097	5	16, 256, 32, 64, 32	3	210	0.00028
12	0.015	5	16, 256, 32, 64, 32	2	100	0.00022
13	0.0153	5	16, 256, 32, 64, 32	3	200	0.000168
14	0.0167	6	16, 32, 128, 16, 128, 256	4	1500	0.000113
15	0.016	4	16, 64, 64, 32	1	400	0.0003
16	0.0077	5	16, 32, 64, 32, 256	4	510	0.00017
17	0.04	3	64, 32, 64	10	520	0.000057
18	0.039	4	16, 256, 256, 32	4	900	0.000018
19	0.02	4	16, 256, 64, 128	6	500	0.000146
20	0.0126	5	16, 256, 32, 64, 128	4	1100	0.0008

Table S4 Performance of models for different dataset sizes. For the forward model, average MSE is used as the performance metric, evaluated on the test dataset. For the inverse model (Tandem), MAE and R-squared values are employed to measure performance, also on the test dataset.

Dataset Size	Inverse Model				Forward Model
4990	Performance Metrics	Thickness	Radius	Periodicity	Average MSE
	MAE (nm)	2.09	1.44	0.986	0.00058
	R-squared value	0.94	0.97	0.977	
6655	MAE (nm)	0.93	1.21	0.56	0.000244
	R-squared value	0.986	0.996	0.996	

Table S5 Performance of models for different cost functions used during training. For the forward model, average MSE is used as the performance metric, evaluated on the test dataset. For the inverse model (Tandem), MAE and R-squared values are employed to measure performance, also on the test dataset.

Cost Function	Inverse Model				Forward Model
MAE	Performance Metrics	Thickness	Radius	Periodicity	Average MSE
	MAE (nm)	1.28	1.5	0.87	0.00064
	R-squared value	0.97	0.99	0.98	
MSE	MAE (nm)	0.93	1.21	0.56	0.000244
	R-squared value	0.986	0.996	0.996	

Table S6 Performance comparison of different dataset sizes on tandem neural network.

Dataset Size	Performance Metrics	Thickness (nm)	Radius (nm)	Periodicity (nm)
6655	MAE	0.93	1.21	0.56
	R^2	0.99	0.99	0.99
7260	MAE	0.96	1.29	0.81
	R^2	0.99	0.99	0.96

Notes and references

1 D. Conteduca, I. Barth, G. Pitruzzello *et al.*, *Nature Communications*, 2021, **12**, 3293.

2 P. B. Johnson and R. W. Christy, *Physical Review B*, 1972, **6**, 4370–4379.

3 E. PALIK, in *Preface*, Elsevier, 1997, p. xvii–xviii.

4 A. Prasad, J. Choi, Z. Jia, S. Park and M. R. Gartia, *Biosensors and Bioelectronics*, 2019, **130**, 185–203.